# Enthalpies of mixing from dilute solutions to high-entropy alloys

Leandro Seixas [1,2,3,*] Raphael M. Tromer,[1] Rafael O. Figueiredo [1] and James M. Almeida[3,4]

[1]*MackGraphe — Mackenzie Institute for Research in Graphene and Nanotechnologies, Mackenzie Presbyterian Institute, Rua da Consolação, 896, São Paulo, São Paulo 01302-907, Brazil*

[2]*Instituto de Física Teórica, Universidade Estadual Paulista, Rua Dr. Bento Teobaldo Ferraz, 271, São Paulo, São Paulo 01140-070, Brazil*

[3]*Ilum — School of Science, Brazilian Center for Research in Energy and Materials (CNPEM), Campinas, São Paulo 13087-548, Brazil*

[4]*Programa de Pós-Graduação em Nanociências e Materiais Avançados, Universidade Federal do ABC, Santo André, São Paulo 09210-580, Brazil*

(Received 3 November 2025; revised 8 September 2026; accepted 3 November 2026; published 17 November 2026)

High-entropy alloys (HEAs) are materials characterized by significant configurational disorder, offering promising properties for mechanical, chemical, and electrochemical applications. However, accurately determining their thermodynamics, especially the enthalpy of mixing, remains challenging because of the complexity of these systems and the limitations of empirical models. Here, we introduce an *ab initio* thermodynamic model that leverages properties of dilute solid solutions to accurately predict the enthalpies of mixing in high-entropy alloys. This approach, called the Dilute Solution Interpolation (DSI) model, shows excellent agreement with experimental data for binary alloys and significantly outperforms semiempirical models like the Miedema model. Furthermore, the model extends to multiprincipal-component alloys, and we demonstrate its application to AgAuCuPdPt, identifying possible phase separations. Our findings reveal that using this model offers a viable alternative for predicting properties from dilute solutions to nearly equimolar alloys and improves the accuracy thermodynamic predictions for HEAs. This advancement offers a more precise framework for designing HEAs, minimizing the reliance on empirical parameters. The study's findings provide fresh insights into thermodynamic modeling and could lead to the development of a wider range of high-performance materials. The model developed here is general and can be extended to other HEAs, including those with different crystalline phases or other materials, such as oxides and other high-entropy compounds, providing a better prediction of HEA crystal phases, especially which compositions could lead to solid solutions. Our results also establish the DSI model's efficiency, characterized by a quadratic $\mathcal{O}(N^2)$ scaling with the number of components ($N$). Consequently, the framework provides a scalable pathway for predicting the properties of concentrated multicomponent alloys.

DOI: 10.1103/pdjg-z6rb

## I. INTRODUCTION

High-entropy alloys (HEAs) [1–4] are a novel class of materials composed of multiple principal components in which the high entropy of mixing induces the formation of single-phase crystalline solid solutions (SS). Unlike traditional alloys, which are typically composed of one or two principal components with minor additions of other elements, HEAs typically consist of five or more principal components mixed in near-equiatomic ratios. These materials exhibit crystalline (geometric) order combined with compositional (chemical) disorder, as illustrated in Fig. 1(a). These materials were independently discovered in 2004 by two research groups. Cantor *et al.* [1] synthesized a solid solution alloy composed of FeMnCoCrNi (Cantor alloy). Meanwhile, Yeh *et al.* [2] discovered a solid solution alloy composed of FeCuCoCrNiAl. In both cases, the alloys possess a face-centered cubic (fcc) lattice crystal structure. Yeh also observed that increasing the Al composition in the alloy leads to a transformation to the body-centered cubic (bcc) crystal phase.

Since its discovery, a plethora of high-entropy alloys have been synthesized and characterized, giving rise to remarkable emergent properties, such as exceptional strength, hardness, corrosion resistance, and thermal stability. These characteristics make them suitable for a broad range of technological applications. In aerospace engineering, HEAs are potential candidates for components such as turbine blades that require high strength and thermal stability at elevated temperatures [6,7]. Furthermore, their high hardness and wear resistance qualify high-entropy alloys as excellent materials for protective coatings on industrial machinery.

Depending on their composition and thermodynamic properties, such as temperature and pressure, these alloys can form (i) multiple phases (MP) that may segregate spatially; (ii) spinodal decomposition (SD); (iii) ordered phases like intermetallic compounds (IM); (iv) amorphous phases such as metallic glasses (MG); or (v) single-phase solid solutions (SS). The differences among these phases are illustrated in Refs. [3,4,8]. A classification of some of these phases is shown by Ye *et al.* [4], based on quantities such as enthalpy of mixing, configurational entropy, valence electron concentration (VEC), and excess configurational entropy.

The phase of the material is determined by the Gibbs free energy of mixing, expressed as

$$\Delta G_{\mathrm{mix}}(\mathbf{X}) = \Delta H_{\mathrm{mix}}(\mathbf{X}) - T\,\Delta S_{\mathrm{mix}}(\mathbf{X}), \tag{1}$$

*Contact author: leandro.s.rocha@unesp.br

 ©2026 American Physical Society

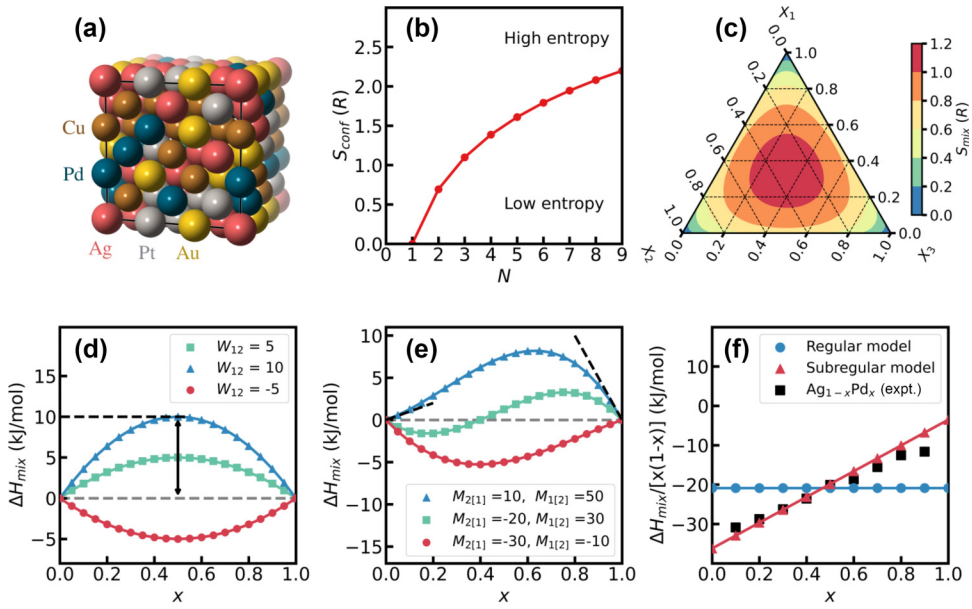



FIG. 1. (a) Schematic representation of a supercell of the high-entropy alloy AgAuCuPdPt with an equimolar composition. (b) Configurational entropy of equimolar alloys with $N$ components. (c) Ternary diagram showing the configurational entropy of a ternary alloy across different compositions. (d) Enthalpy of mixing for binary alloys using the regular solution model. The curves depict various values of the $W_{12}$ parameter. The value of the $W_{12}$ parameter is indicated by the height marked by the black dashed line. (e) Enthalpy of mixing for binary alloys using the subregular solution model. The various curves illustrate different relationships between the differential mixing enthalpies $M_{2[1]}$ and $M_{1[2]}$. The black dashed lines indicate the slopes of the tangent lines for the enthalpy of mixing at the dilution limits ($x \approx 0$ and $x \approx 1$). (f) Comparison of the regular solution model, subregular solution model, and experimental data for the $Ag_{1-x}Pd_x$ binary alloy [5].

where $\Delta H_{\text{mix}}$ represents the enthalpy of mixing, $\Delta S_{\text{mix}}$ represents the entropy of mixing, and $T$ is the absolute temperature. $\mathbf{X}$ is a vector in the compositional space (simplex space), with components given by the molar fractions $X_i$, with $0 \leqslant X_i \leqslant 1$ and $\sum X_i = 1$. For the alloy to form a stable solid solution, $\Delta G_{\text{mix}}$ must be a convex function of $X$. Regions of concavity in the $\Delta G_{\text{mix}}(\mathbf{X})$ result in instabilities that induce segregation into multiple phases [9]. For the binary alloy, the Gibbs free energy is a function of a single molar fraction ($x$), and the convex hull condition is given by

$$\Delta G_{\text{mix}}(x) \geqslant \Delta G_{\text{mix}}(x_0) + (x - x_0) \left. \frac{\mathrm{d}\Delta G_{\text{mix}}}{\mathrm{d}x} \right|_{x_0}, \qquad (2)$$

for any $x_0$ in the compositional space.

The spinodal decomposition is also obtained directly from the $\Delta G_{\text{mix}}$. For a binary alloy, the region of the phase diagram for the spinodal decomposition is given by $\frac{\mathrm{d}^2 \Delta G_{\text{mix}}}{\mathrm{d}x^2} \leqslant 0$, with the spinodal curve given by setting this second-order derivative to zero [10].

The entropy of mixing is approximated here by the ideal configurational entropy, given by

$$S_{\text{conf}}(\mathbf{X}) = -R \sum_{i=1}^{N} X_i \ln(X_i), \qquad (3)$$

where $R = 8.314\ 462\ 618\ \text{J mol}^{-1}\ \text{K}^{-1}$ is the universal gas constant (CODATA exact value) [11]. This configurational entropy reaches its maximum for equimolar compositions. Another important term in the entropy of mixing, especially at high temperatures, is the excess vibrational entropy, which is not taken into account in models in the literature and is usually not evaluated using *ab initio* methodologies even when considered. For equimolar alloys with $N$ components, the configurational entropy is given by $S_{\text{conf}} = R \ln(N)$ as illustrated in Fig. 1(b). One way to classify high-entropy alloys is based on their configurational entropy. This classification divides alloys into low-entropy ($S_{\text{conf}} < R$), medium-entropy ($R \leqslant S_{\text{conf}} < 1.5R$), and high-entropy ($S_{\text{conf}} \geqslant 1.5R$).

It is important not to define strict thresholds for configurational entropy when generalizing this class of materials to include different compositions and crystal structures. Here, we define a high-entropy alloy as a material where the mixing entropy favors the formation of solid solutions with a single-phase crystalline structure. In this new framework, the enthalpy of mixing becomes critical, and semiempirical models such as the Miedema [12] or CALPHAD [13] models become limiting factors for discovering and designing novel high-entropy alloys. In Fig. 1(c), it is shown that the configurational entropy of a ternary alloy varies significantly with composition, peaking at the equimolar composition. For the $N$ components alloy, the configurational entropy will be maximal when the molar fractions are $X_i = 1/N$.

The enthalpy of mixing in high-entropy alloys is typically determined using a solution model that aggregates the contributions from pairs of components that create binary alloys [4,14],

$$\Delta H_{\text{mix}}(\mathbf{X}) = \sum_{i=1}^{N-1} \sum_{j=i+1}^{N} \Omega_{ij} X_i X_j, \qquad (4)$$

where $N$ represents the number of components in the alloy, and $\Omega_{ij}$ is the interaction parameter of the solution. The simplest solution model is the regular solution model. In this

model, the interaction parameters are defined as $\Omega_{ij} = 4W_{ij}$, where $W_{ij}$ are constants.

For a binary alloy, the enthalpy of mixing according to the regular solution model is given by

$$\Delta H^{R}_{\text{mix}}(x) = 4W_{12}x(1-x), \tag{5}$$

where $x$ represents the concentration of one of the alloy's components. The superscript index $R$ denotes the approximation of the enthalpy of mixing according to the regular solution model. Specifically, for an equimolar binary alloy ($x = \frac{1}{2}$), the equation simplifies to $\Delta H^{R}_{\text{mix}}(x)|_{x=\frac{1}{2}} = W_{12}$. Thus, the parameter $W_{12}$ can be interpreted as the enthalpy of mixing at $x = \frac{1}{2}$, as illustrated in Fig. 1(d).

The parameter $W_{ij}$ in the regular solution model can be estimated using empirical data, semiempirical models (such as the Miedema model), or *ab initio* calculations such as those based on density functional theory (DFT). To model the disorder within alloys in a supercell, the cluster expansion (CE) [17,18] or special quasirandom structures (SQS) method [19–23] are used. The CE method combines interaction patterns between components with energy contributions from multiple orders of defined configurations, calculated using first-principles methods. The SQS method seeks to create relatively small supercells that effectively represent optimized local disorder by matching the correlation functions between components. Both the CE and SQS methods have been extensively applied to the study of low-entropy alloy formation [24,25].

In this work, we propose a model for element mixing in high-entropy alloys, with parameters derived from the *ab initio* thermodynamics of dilute solutions. For a high-entropy alloy with $N$ components, we demonstrate that the enthalpy of mixing across the compositional space is determined by $N^2$ parameters, each calculated from *ab initio* simulations of dilute binary solutions. We apply this model to compute the enthalpy of mixing for the quinary ($N = 5$) high-entropy alloy AgAuCuPdPt, which is currently being explored for applications in areas such as catalysis and chemical sensing.

Noble-metal HEAs have emerged as versatile platforms for catalysis and electrocatalysis [26–29]. The vast compositional space and synergistic "cocktail" effects [30] allow for precise tuning of surface adsorption energies, significantly enhancing reaction kinetics across various applications. Consequently, noble-metal HEA nanoparticles have demonstrated exceptional performance in reactions such as hydrogen and oxygen evolution [31–34], nitrogen reduction [35], and complex organic oxidations [36,37].

Despite the immense interest in these materials, fundamental questions regarding their structural stability remain elusive. For instance, the phase behavior of the AgAuCuPdPt HEA is currently debated in the literature. While Sohn *et al.* [38] found that introducing Cu into the single-phase fcc AgAuPdPt alloy causes phase separation into two distinct fcc structures, subsequent studies on AgAuCuPdPt nanoparticles [39,40] reported a single-phase solid solution. These conflicting observations necessitate a systematic thermodynamic study of the bulk AgAuCuPdPt alloy to establish its intrinsic phase stability and to disentangle bulk properties from nanoscale confinement and surface effects.

## II. METHODS

We performed *ab initio* calculations utilizing density functional theory [41,42] as implemented in the GPAW (Grid-based Projector-Augmented Wave) code [43]. These simulations used a plane-wave basis with a cutoff energy of 900 eV [44]. An analysis of the convergence of the total energy with the cutoff energy is shown in Fig. S7 within the Supplemental Material (SM) [45]. The exchange-correlation functional was applied in the generalized gradient approximation, using the Perdew–Burke–Ernzerhof (PBE) parametrization [46]. The k-point grid was set to $15 \times 15 \times 15$, employing the Monkhorst–Pack algorithm [47] for the unit cell. All geometries were fully optimized to meet a force criterion of less than 0.02 eV/Å, including unit-cell relaxation.

The calculations were performed on a supercell of $3 \times 3 \times 3$ primitive cells, resulting in a total of 27 atoms in the supercell. This supercell size was chosen to ensure that the dilute solution approximation is valid, as it allows for the substitution of one atom with another element while maintaining a sufficiently low concentration of the solute ($x_0 = 1/27$).

## III. RESULTS AND DISCUSSION

The model for the enthalpy of mixing for $N$ components proposed in this paper is based on modifying the interaction parameter $\Omega_{ij}$, in Eq. (4). We propose that the interaction parameter should be expressed as follows:

$$\Omega^{\sigma}_{ij} = (M_{j[i]}X_i + M_{i[j]}X_j)/(X_i + X_j + \varepsilon), \tag{6}$$

where $M_{j[i]}$, referred to as the differential mixing enthalpy, can be calculated using *ab initio* methods of dilute binary solutions. The parameters for the *ab initio* simulations are shown in Sec. II. $\varepsilon$ is a small positive constant added to prevent division by zero. A convergence threshold of $\varepsilon = 10^{-8}$ was employed; further reduction of this parameter did not alter the results, ensuring numerical stability. The model described by the equation above is referred to as a subregular solution model, having already been applied to experimental data from both binary and multicomponent alloys [5,48]. The superscript $\sigma$ denotes the approximation of the enthalpy of mixing obtained using the subregular solution model.

To better understand the parameters $M_{i[j]}$ and $M_{j[i]}$, we examine the model for binary alloys. In this context, the enthalpy of mixing for subregular solutions can be expressed as

$$\Delta H^{\sigma}_{\text{mix}}(x) = M_{2[1]}x(1-x)^2 + M_{1[2]}x^2(1-x). \tag{7}$$

Figure 1(e) illustrates examples of enthalpies of mixing with different values of $M_{i[j]}$. For positive $M_{1[2]}$ and $M_{2[1]}$, the enthalpies of mixing remain nonnegative for any value of $x$. However, unlike the regular solution model, the maximum enthalpy of mixing does not always occur at $x = 1/2$; it can shift depending on the ratio between $M_{1[2]}$ and $M_{2[1]}$. When both differential mixing enthalpies are negative, the enthalpies of mixing are nonpositive for all values of $x$. Similarly, when the dilution strengths are positive, the enthalpies of mixing are nonnegative across all compositions. An intriguing scenario arises when the differential mixing enthalpies $M_{1[2]}$ and $M_{2[1]}$ have opposite signs. In this case, the enthalpy of mixing can change sign as the concentration changes, as illustrated

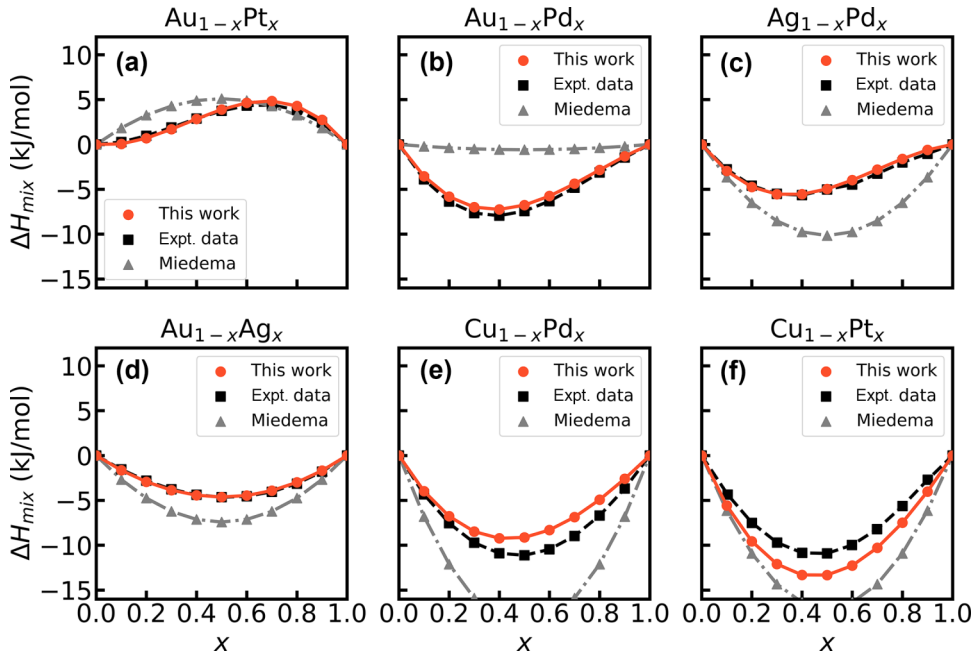



FIG. 2. Enthalpy of mixing for binary alloys. (a) $Au_{1-x}Pt_x$, (b)$Au_{1-x}Pd_x$, (c) $Ag_{1-x}Pd_x$, (d) $Au_{1-x}Ag_x$, (e) $Cu_{1-x}Pd_x$, and (f) $Cu_{1-x}Pt_x$. Our model predictions are shown as orange filled circles, the Miedema model predictions are shown as gray triangles, and the experimental data are shown as black squares [5,15,16].

in Fig. 1(e). This results in some concentrations exhibiting endothermic enthalpies, while others show exothermic enthalpies.

In the limit of dilute solutions, where $x \approx 0$ and $x \approx 1$, the derivatives of the mixing enthalpy are given by [49]

$$M_{2[1]} = \left.\frac{\mathrm{d}\Delta H^{\sigma}_{\mathrm{mix}}}{\mathrm{d}x}\right|_{x=0}, \quad M_{1[2]} = -\left.\frac{\mathrm{d}\Delta H^{\sigma}_{\mathrm{mix}}}{\mathrm{d}x}\right|_{x=1}. \tag{8}$$

In other words, the parameters $M_{i[j]}$ represent how the enthalpies of mixing change with the concentration of each component. Specifically, $M_{i[j]}$ indicates the change in $\Delta H^{\sigma}_{\mathrm{mix}}$ when component $i$ (solute) is dissolved in component $j$ (solvent). The tangent lines corresponding to the derivatives of $\Delta H^{\sigma}_{\mathrm{mix}}$ are depicted in Fig. 1(e) as black dashed lines.

Comparing the regular and subregular mixture models with experimental data, we can examine the behavior of the quantity $\Delta H_{\mathrm{mix}}/[x(1-x)]$. In the regular solution model, this quantity remains constant and is equal to $W_{12}$. However, in the subregular solution model, it forms a straight line determined by the parameters $M_{2[1]}$ and $M_{1[2]}$. When compared to experimental data for the binary alloy $Ag_{1-x}Pd_x$ [5], the subregular solution model shows excellent agreement with the experimental results, as shown in Fig. 1(f).

The $M_{i[j]}$ are derived from the total enthalpy of mixing,

$$\Delta h_{\mathrm{mix}}(x) = E(A_{1-x}B_x) - [(1-x)E(A) + xE(B)], \tag{9}$$

where $E(Z)$ is the total energy of system $Z = A$, $B$, or $A_{1-x}B_x$. In the dilute limit ($x \approx 0$), we find that

$$M_{2[1]} = \Delta h_{\mathrm{mix}}(x = 1/N). \tag{10}$$

Following a similar procedure, the $M_{1[2]}$ parameter is extracted from the mixing enthalpy in the dilute limit of the second component ($x \approx 1$).

Although the parameters $M_{2[1]}$ and $M_{1[2]}$ are determined within the dilute solution regimes, the subregular solution model using these parameters remains valid across the entire concentration range in the compositional space. The enthalpy of mixing for values of $x$ outside the dilute region is obtained by interpolating the model using parameters $M_{2[1]}$ and $M_{1[2]}$. Thus, we refer to our approach as the dilute solution interpolation (DSI) model. An analogous procedure was detailed by Benisek and Dachs for evaluating the enthalpy of mixing in binary mineral solid solutions [50].

We apply our model to calculate the differential mixing enthalpies $M_{i[j]}$ and $M_{j[i]}$ for the binary alloys $Au_{1-x}Pt_x$, $Au_{1-x}Pd_x$, $Ag_{1-x}Pd_x$, $Au_{1-x}Ag_x$, $Cu_{1-x}Pd_x$, and $Cu_{1-x}Pt_x$. These binary alloys were selected because of the availability of experimental data on enthalpies of mixing for solid solutions, as reported in Refs. [5,15,16,51,52]. We can also compare our results with predictions from the Miedema model [12]. The results are presented in Fig. 2. Our model shows exceptional agreement with the experimental data, particularly for the $Au_{1-x}Pt_x$, $Au_{1-x}Pd_x$, $Ag_{1-x}Pd_x$, and $Au_{1-x}Ag_x$ alloys. For the $Cu_{1-x}Pd_x$ and $Cu_{1-x}Pt_x$, the agreement is still excellent. The $M_{i[j]}$ parameters for all binary alloys calculated in this study are presented in Table S1 within the SM [45]. While the Miedema model is used in the literature to predict the enthalpies of mixing for high-entropy alloys [12,53], it does not quantitatively match the experimental data for most of the alloys examined in this study. The model developed in this work is expected to significantly enhance the accuracy of predictions for the thermodynamic properties of novel high-entropy alloys.

Using the data from our model, the Miedema model, and experimental results, we can calculate the root-mean-square error (RMSE) for these alloys. With the model developed here, the RMSE is less than 2 kJ/mol for the binary alloys

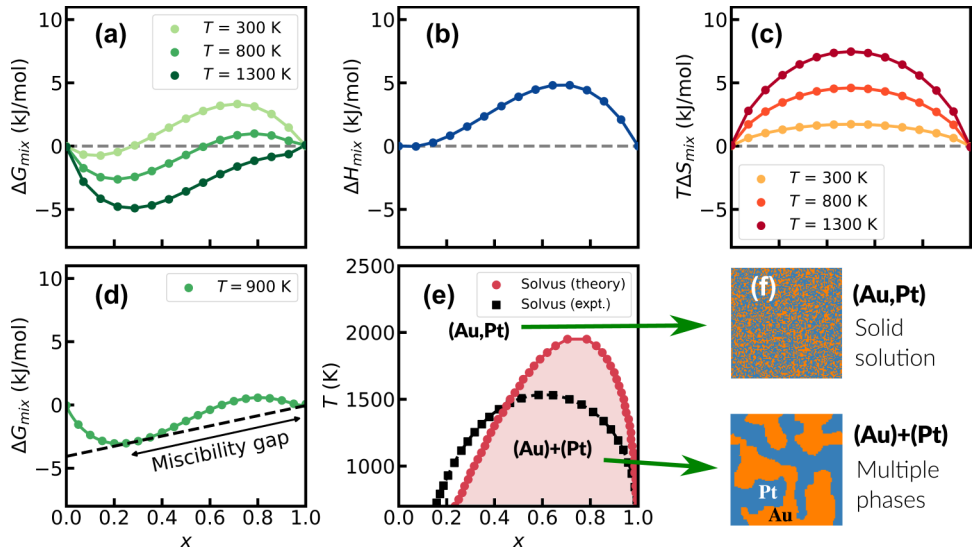



FIG. 3. Binary alloy $Au_{1-x}Pt_x$. (a) Gibbs free energy of mixing for three different temperatures (300 K, 800 K, and 1300 K). (b) Enthalpy of mixing from first-principles calculations based on our model. (c) Entropy of mixing (configurational entropy) times temperature for three different temperatures (300 K, 800 K, and 1300 K). (d) Convexity analysis of Gibbs free energy of mixing for $T = 900$ K. Between $x = 0.28$ and $x = 0.99$, the curve is connected by the Maxwell construction to maintain the convexity of the Gibbs free energy. In this region, there is a separation into multiple phases. (e) Phase diagram and solvus curve for $Au_{1-x}Pt_x$ with experimental data and with our theoretical model. (f) Schematic representation of a solid solution (Au, Pt) and multiple phases (Au)+(Pt).

studied, while the RMSE for the Miedema model can exceed 5 kJ/mol. These comparisons are detailed in the SM (Fig. S1) [45]. The model was also applied to other binary alloys, including $Au_{1-x}Cu_x$, $Ag_{1-x}Cu_x$, $Ag_{1-x}Pt_x$, and $Pd_{1-x}Pt_x$. Comparisons of the enthalpies of mixing for these alloys with those predicted by the Miedema model are provided in the SM (Fig. S2) [45].

It is important to emphasize that the model developed here is more general than the specific compositions and structures investigated in this study. This model can be applied to composite materials with alloyed sublattices. Beyond medium- and high-entropy alloys, other high-entropy materials are gaining attention in the literature, including oxides [54], carbides [55], silicides [56], halides [57], and sulfides [58,59]. While experimental data and semiempirical models for these high-entropy compounds are currently lacking, our model can be used to calculate their mixing enthalpies using first-principles simulations. As a result, this model is poised to become a valuable tool for guiding the discovery and design of novel high-entropy materials.

The predictive capability of our DSI model extends well beyond the noble-metal systems investigated in this study. Refractory alloys, specifically the MoWNbTa system, represent a highly promising avenue for further application. To support this, the SM [45] details the calculated enthalpies of mixing for the relevant binary (MoNb, MoTa, MoW, NbTa, NbW, TaW) SM [45] and ternary (MoNbTa) subsystems (Figs. S3 and S4, respectively) SM [45], including a systematic benchmark against the Miedema model. To assess the model's performance in nonmetallic systems, we applied it to the covalently bonded SiGe binary system (Fig. S5 within the SM [45]). The calculated values show excellent agreement with experimental measurements from Ref. [60], demonstrating the model's applicability to a broader range of materials beyond metallic alloys.

In our computational model, we use supercells consisting of $3 \times 3 \times 3$ primitive fcc cells, with 27 atoms per unit cell. Substitutional defects were introduced to calculate the mixing enthalpy.

From the enthalpies of mixing and the configurational entropy, other thermodynamic properties can be derived. For instance, the Gibbs free energy as a function of concentration, $\Delta G_{\mathrm{mix}}(x)$, can be calculated. Figure 3(a) shows the Gibbs free energy for the binary alloy $Au_{1-x}Pt_x$ at three different temperatures (300 K, 800 K, and 1300 K). The enthalpy of mixing, calculated using the model developed in this work, is displayed in Fig. 3(b). Meanwhile, the product of the configurational entropy and temperature is illustrated in Fig. 3(c) for the same three temperatures.

As the temperature increases, the Gibbs free energies become more negative and exhibit greater convexity. The concave region of the Gibbs free energy is defined by the bitangent line, as shown in Fig. 3(d). For the Gibbs free energy at 900 K, we observe that the solid solution is stable between $x = 0$ and $x = 0.28$, as well as between $x = 0.99$ and $x = 1.0$. In the concentration range from $x = 0.28$ to $x = 0.99$, the solid solution, represented as (Au, Pt), is unstable, and the system undergoes phase separation into two phases, denoted as (Au)+(Pt). This region of the compositional space, where the solid solution is not stable, is known as the miscibility gap.

By calculating the miscibility gap at various temperatures, we can derive the solvus curve from our model. When compared to the experimental solvus of the $Au_{1-x}Pt_x$ alloy, we find good agreement for temperatures below 1000 K. However, at higher temperatures, the theoretical solvus begins to deviate from the experimental data. This divergence is primarily due

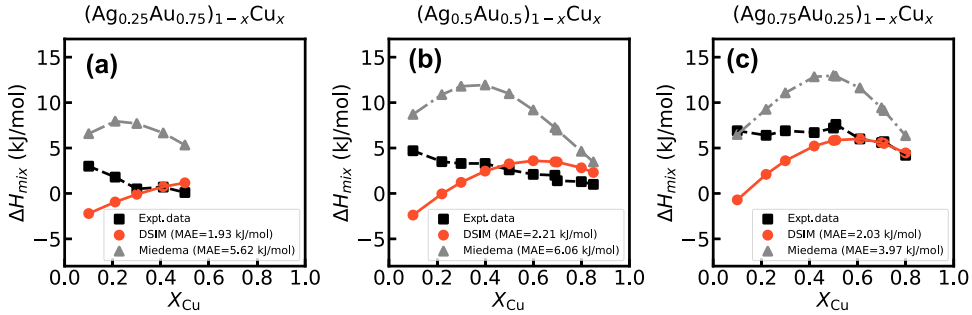



FIG. 4. Enthalpy of mixing for the ternary alloy AgAuCu. (a) $X_{Ag}/X_{Au} = 1/3$, (b) $X_{Ag}/X_{Au} = 1$, and (c) $X_{Ag}/X_{Au} = 3$. The DSI model is shown as orange filled circles, the Miedema model is shown as gray triangles, and the experimental data are shown as black squares [61].

to the approximation of the entropy of mixing by configurational entropy. At elevated temperatures, vibrational entropy makes significant contributions to the entropy of mixing, as predicted by Senkov and Miracle [62]. A more detailed investigation of vibrational entropy and other components of the entropy should be undertaken in future work.

To validate our approach, the mixing enthalpies of the ternary AgAuCu system were calculated and compared with both experimental data [61] and the Miedema model [61,63]. As illustrated in Fig. 4, the DSI model provides a significant improvement in predicting $\Delta H_{mix}$ for this ternary system. The data are categorized by the silver-to-gold ratio, specifically (a) $X_{Ag}/X_{Au} = 1/3$, (b) $X_{Ag}/X_{Au} = 1$, and (c) $X_{Ag}/X_{Au} = 3$, with the Cu concentration ($x$) treated as the independent variable. While the DSI model exhibits excellent agreement for $x \gtrsim 0.3$, minor deviations from experimental values are observed at lower Cu concentrations. Quantitatively, the DSI model yields a mean absolute error (MAE) of approximately 2 kJ/mol, whereas the Miedema model's error reaches 6 kJ/mol. These results suggest that the DSI framework is robustly applicable to complex multicomponent systems, including high-entropy alloys. At low copper concentrations, our model exhibits notable deviations from the experimental data. These discrepancies likely stem from the mismatch in the covalent radii of Cu relative to Au and Ag, which induces local lattice distortions not captured by the present model. Consistent with this hypothesis, Cu-containing binary alloys also display the most pronounced deviations from experimental observations, as shown in Fig. 2. A detailed investigation of these lattice effects is deferred to future work.

For multicomponent systems, we determine the total enthalpy of mixing by aggregating the contributions from the

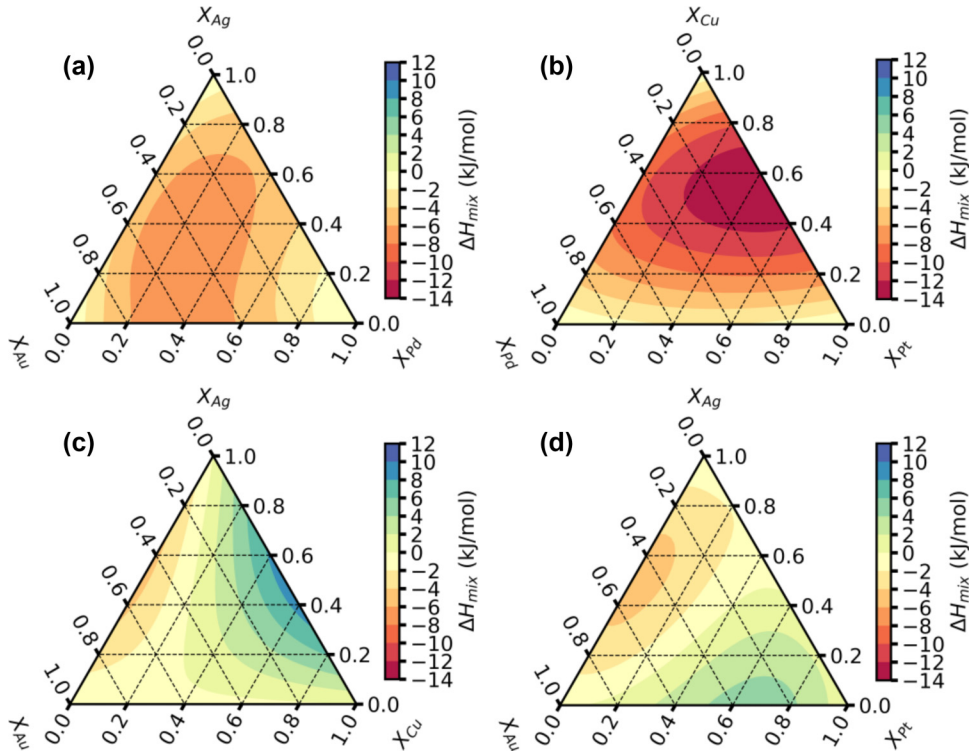



FIG. 5. Enthalpy of mixing for ternary alloys. (a) AgAuPd, (b) CuPdPt, (c) AgAuCu, and (d) AuAgPt. Compositions with low enthalpies of mixing are shown in red, while those with high enthalpies of mixing are displayed in blue.

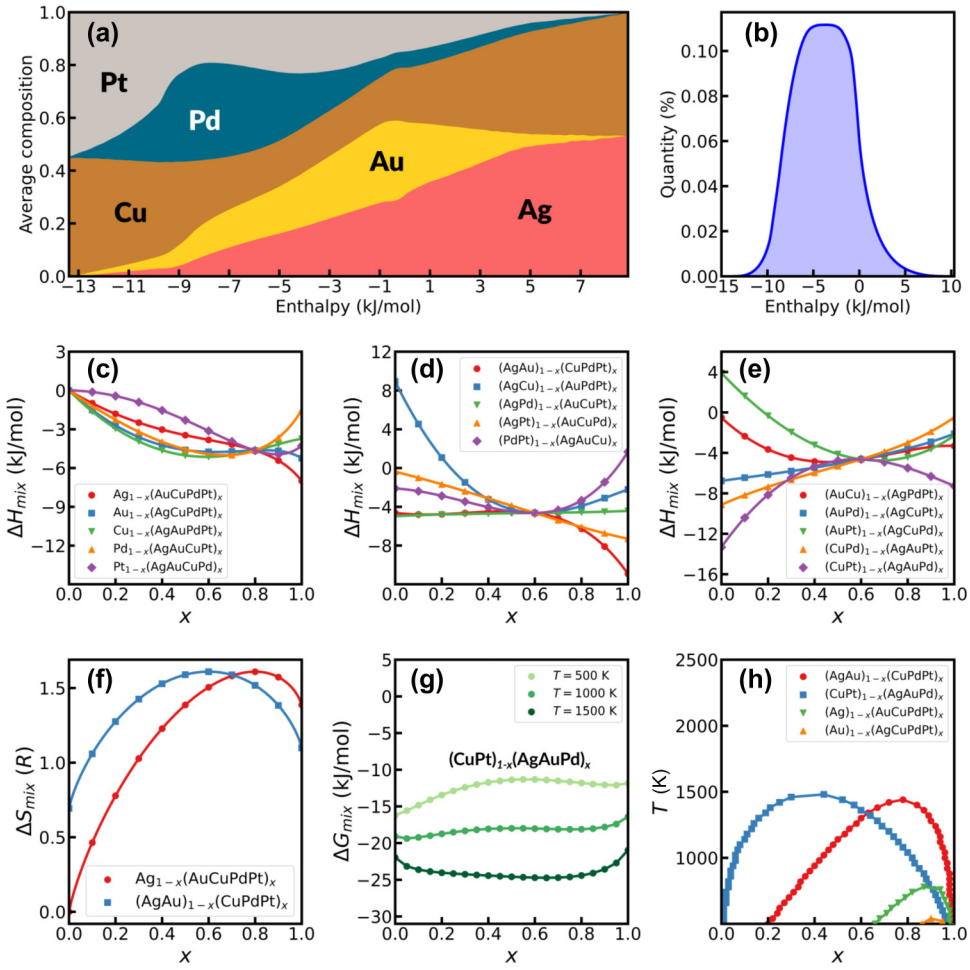



FIG. 6. Thermodynamic properties of high-entropy alloys. (a) Average composition of AgAuCuPdPt alloys for each enthalpy of mixing value. (b) Distribution of high-entropy alloy compositions as a function of enthalpy of mixing. (c)–(e) Changes in mixing enthalpy with the addition of one element (c) or two elements (d)(e). (f) Variation in mixing entropy with the addition of one or two components. (g) Gibbs free energy variation for the alloy $(CuPt)_{1-x}(AgAuPd)_x$ at three different temperatures. (h) Theoretical solvus curves for AgAuCuPdPt-based high-entropy alloys with varying compositions.

underlying binary subsystems. In Fig. 5, we present ternary plots for the following ternary alloys: (a) AgAuPd, (b) CuPdPt, (c) AgAuCu, and (d) AuAgPt. The molar concentrations at which the mixing enthalpies are more negative (positive) are shown in red (blue). Results for other ternary alloys are provided in the SM (Fig. S6) [45]. We observe that the components Ag, Au, and Pd are highly miscible, forming stable ternary solid solutions (Ag, Au, Pd). Moreover, the components Cu, Pd, and Pt are highly miscible with each other, as indicated by the negative mixing enthalpies for various compositions of this ternary alloy. This miscibility is expected to promote the formation of (Cu, Pd, Pt) solid solutions.

In contrast, the Cu component is highly immiscible with Ag, and the Pt component is highly immiscible with Au, as indicated by the blue regions in Figs. 5(c) and 5(d), respectively. Combining these results, we expect phase separations between (Ag, Au, Pd)-rich and (Cu, Pt, Pd)-rich phases. This difference in miscibility helps explain the results observed by Sohn *et al.* [38], who reported the duplication of the fcc crystalline phase upon the incorporation of Cu into the AgAuPdPt alloy, suggesting an enthalpic origin for phase segregation. The single phase observed by Nellaiappan *et al.* [39] and Urs *et al.* [40] likely arises from diffusion restrictions caused by lattice distortions, surface effects, or quantum confinement in the metal nanoparticles.

By calculating the enthalpies of mixing for all possible proportions of Ag, Au, Cu, Pd, and Pt, with 1% increments for each component, we can group compositions with similar values. We can determine the average compositions corresponding to each enthalpy value, as shown in Fig. 6(a). Compositions that are rich in Cu and Pt, but low in Ag, Au, and Pd, exhibit the lowest mixing enthalpies and tend to form solid solutions. In contrast, compositions rich in Ag and Cu, but poor in Au, Pd, and Pt, show the highest enthalpies of mixing, indicating a tendency to form multiple phases. The distribution of the number of compositions corresponding to each enthalpy of mixing is represented by the smoothed histogram in Fig. 6(b). The majority of compositions have mixing enthalpies around –5 kJ/mol. This indicates that, in

general, the components Ag, Au, Cu, Pd, and Pt are largely miscible in high-entropy alloys, even at low temperatures when entropic effects are minimal.

Another approach to analyzing the enthalpies of mixing of high-entropy alloys is to apply constraints that limit our compositional space to a few specific lines. For these alloys, we calculate both the enthalpies of mixing and configurational entropy, as shown in Figs. 6(c)–6(f). In Fig. 6(c), equimolar quaternary alloys are maintained at equal concentrations of four components while a fifth component is added. Figures 6(d) and 6(e) show how binary alloy compositions are included within ternary alloys. Figure 6(f) presents the configurational entropy for the concentration variations depicted in Figs. 6(c)–6(e).

In this analysis, the Gibbs free energy is computed at various temperatures to examine its convexity and assess the potential for phase segregation in high-entropy alloys, as illustrated in Fig. 6(g). By exploring these variations under constraints on the proportions, we find that the primary phase segregations in this high-entropy alloy are likely to be either (Ag, Au)+(Cu, Pd, Pt) or (Ag, Au, Pd)+(Cu, Pt), as indicated by the theoretical solvus curves shown in Fig. 6(h).

To illustrate the practical efficiency of our approach, consider a quinary alloy ($N = 5$) such as those investigated in this work. Within the DSI framework, the enthalpy of mixing across the entire compositional space is fully determined by only $N^2 = 25$ *ab initio* simulations. Even for alloys with many more components, our framework demonstrates that it is possible to calculate mixing enthalpies in a scalable manner.

## IV. CONCLUSIONS

In summary, we have developed a model (Dilute Solution Interpolation model) and methodology to determine the enthalpies of mixing of high-entropy alloys using *ab initio* calculations. These enthalpies, interpolated from dilute solution data, show excellent agreement with experimental data for noble-metal alloys such as AuPt, AuPd, AgPd, AgAu, CuPd, and CuPt. The results also exhibit strong agreement with experimental data for the AgAuCu ternary alloy. Based on these enthalpies of mixing, we have classified phases as solid solutions or multiple phases for high-entropy binary and quinary alloys. Additionally, our model has helped elucidate the phase doubling observed in the high-entropy alloy AgAuCuPdPt by Sohn *et al.* [38], identifying possible phase separations such as (Ag,Au)+(Cu, Pd, Pt) or (Ag, Au, Pd)+(Cu, Pt).

The model developed here is general and can be extended to other high-entropy alloys, including those with different crystalline phases or other materials, such as oxides and other high-entropy compounds. Predicting these thermodynamic properties from *ab initio* simulations can provide valuable guidance for discovering and designing solid-solution-forming high-entropy alloys, potentially uncovering new emergent properties in these complex materials.

For high-entropy alloys with many chemical species, the DSI model provides a robust and efficient pathway for enthalpy predictions that would otherwise be numerically inaccessible.

## ACKNOWLEDGMENTS

We thank the funding agencies Conselho Nacional de Desenvolvimento Científico e Tecnológico (CNPq) (Grants No. 308928/2023-7 and No. 308403/2025-8), INCT Materials Informatics (Grant No. 406447/2022-5), and Fundação de Amparo a Pesquisa do Estado de São Paulo (FAPESP) (Grants No. 22/14549-3, No. 23/15372-2, No. 23/13081-0, No. 23/09820-2, and No. 25/09430-5). We also thank Centro Nacional de Processamento de Alto Desempenho em São Paulo (CENAPAD-SP) for providing computational facilities.

## DATA AVAILABILITY

The data that support the findings of this study are available from the corresponding author upon reasonable request.

[1] B. Cantor, I. Chang, P. Knight, and A. Vincent, Microstructural development in equiatomic multicomponent alloys, Mater. Sci. Eng. A **375-377**, 213 (2004).

[2] J.-W. Yeh, S.-K. Chen, S.-J. Lin, J.-Y. Gan, T.-S. Chin, T.-T. Shun, C.-H. Tsau, and S.-Y. Chang, Nanostructured high-entropy alloys with multiple principal elements: Novel alloy design concepts and outcomes, Adv. Eng. Mater. **6**, 299 (2004).

[3] E. P. George, D. Raabe, and R. O. Ritchie, High-entropy alloys, Nat. Rev. Mater. **4**, 515 (2019).

[4] Y. Ye, Q. Wang, J. Lu, C. Liu, and Y. Yang, High-entropy alloy: Challenges and prospects, Mater. Today **19**, 349 (2016).

[5] T. Tanaka, N. A. Gokcen, C. K. Kumar, S. Hara, and Z.-i. Morita, Thermodynamic relationship between enthalpy of mixing and excess entropy in solid solutions of binary alloys, Z. Metallkd. **87**, 779 (1996).

[6] J. H. Perepezko, The hotter the engine, the better, Science **326**, 1068 (2009).

[7] M. Dada, P. Popoola, and N. Mathe, Recent advances of high entropy alloys for aerospace applications: A review, World J. Eng. **20**, 43 (2023).

[8] Y. Ye, Q. Wang, J. Lu, C. Liu, and Y. Yang, The generalized thermodynamic rule for phase selection in multicomponent alloys, Intermetallics **59**, 75 (2015).

[9] S. J. McCormack and A. Navrotsky, Thermodynamics of high entropy oxides, Acta Mater. **202**, 1 (2021).

[10] E. Favvas and A. C. Mitropoulos, What is spinodal decomposition? J. Eng. Sci. Technol. Rev. **1**, 25 (2008).

[11] E. Tiesinga, P. J. Mohr, D. B. Newell, and B. N. Taylor, CODATA recommended values of the fundamental physical constants: 2018, Rev. Mod. Phys. **93**, 025010 (2021).

[12] A. Miedema, R. Boom, and F. De Boer, On the heat of formation of solid alloys, J. Less-Common Met. **41**, 283 (1975).

[13] W. Chen, A. Hilhorst, G. Bokas, S. Gorsse, P. J. Jacques, and G. Hautier, A map of single-phase high-entropy alloys, Nat. Commun. **14**, 2856 (2023).

[14] J. Morral and S. Chen, A regular solution model for a single-phase high entropy and enthalpy alloy, J. Phase Equilib. Diffus. **38**, 382 (2017).
[15] H. Okamoto and T. Massalski, The Au-Pt (Gold-Platinum) system, Bull. Alloy Phase Diagrams **6**, 46 (1985).
[16] H. Okamoto and T. Massalski, The Au-Pd (Gold-Palladium) system, Bull. Alloy Phase Diagrams **6**, 229 (1985).
[17] S. Kadkhodaei and J. A. Muñoz, Cluster expansion of alloy theory: A review of historical development and modern innovations, JOM **73**, 3326 (2021).
[18] J. M. Sanchez, F. Ducastelle, and D. Gratias, Generalized cluster description of multicomponent systems, Physica A **128**, 334 (1984).
[19] A. Zunger, S.-H. Wei, L. Ferreira, and J. E. Bernard, Special quasirandom structures, Phys. Rev. Lett. **65**, 353 (1990).
[20] S.-H. Wei, L. Ferreira, J. E. Bernard, and A. Zunger, Electronic properties of random alloys: Special quasirandom structures, Phys. Rev. B **42**, 9622 (1990).
[21] M. C. Gao, C. Niu, C. Jiang, and D. L. Irving, Applications of special quasi-random structures to high-entropy alloys, in *High-Entropy Alloys: Fundamentals and Applications* (Springer, New York, 2016), pp. 333–368.
[22] V. Sorkin, S. Chen, T. L. Tan, Z. Yu, M. Man, and Y. Zhang, First-principles-based high-throughput computation for high entropy alloys with short range order, J. Alloys Compd. **882**, 160776 (2021).
[23] M. Karabin, W. R. Mondal, A. Östlin, W.-G. D. Ho, V. Dobrosavljevic, K.-M. Tam, H. Terletska, L. Chioncel, Y. Wang, and M. Eisenbach, *Ab initio* approaches to high-entropy alloys: A comparison of CPA, SQS, and supercell methods, J. Mater. Sci. **57**, 10677 (2022).
[24] V. Ozoliņš, C. Wolverton, and A. Zunger, Cu-Au, Ag-Au, Cu-Ag, and Ni-Au intermetallics: First-principles study of temperature-composition phase diagrams and structures, Phys. Rev. B **57**, 6427 (1998).
[25] J. Zhang, S. Zhang, X. Xu, and L. Zhang, First-principles calculation of Fe-Mo-Cr alloys based on special quasi-random structure, Mater. Today Commun. **35**, 106179 (2023).
[26] Y. Xin, S. Li, Y. Qian, W. Zhu, H. Yuan, P. Jiang, R. Guo, and L. Wang, High-entropy alloys as a platform for catalysis: Progress, challenges, and opportunities, ACS Catal. **10**, 11280 (2020).
[27] Z. Wang, J. You, Y. Zhao, R. Yao, G. Liu, J. Lu, and S. Zhao, Research progress on high entropy alloys and high entropy derivatives as OER catalysts, J. Environ. Chem. Engn. **11**, 109080 (2023).
[28] A. Ostovari Moghaddam and E. A. Trofimov, Toward expanding the realm of high entropy materials to platinum group metals: A review, J. Alloys Compd. **851**, 156838 (2021).
[29] Y.-C. Qin, F.-Q. Wang, X.-M. Wang, M.-W. Wang, W.-L. Zhang, W.-K. An, X.-P. Wang, Y.-L. Ren, X. Zheng, D.-C. Lv, and A. Ahmad, Noble metal-based high-entropy alloys as advanced electrocatalysts for energy conversion, Rare Metals **40**, 2354 (2021).
[30] L. Wang, L. Zhang, X. Lu, F. Wu, X. Sun, H. Zhao, and Q. Li, Surprising cocktail effect in high entropy alloys on catalyzing magnesium hydride for solid-state hydrogen storage, Chem. Eng. J. **465**, 142766 (2023).
[31] Q. Zhang, K. Lian, Q. Liu, G. Qi, S. Zhang, J. Luo, and X. Liu, High entropy alloy nanoparticles as efficient catalysts for alkaline overall seawater splitting and Zn-air batteries, J. Colloid Interface Sci. **646**, 844 (2023).
[32] T. A. Batchelor, J. K. Pedersen, S. H. Winther, I. E. Castelli, K. W. Jacobsen, and J. Rossmeisl, High-entropy alloys as a discovery platform for electrocatalysis, Joule **3**, 834 (2019).
[33] D. Wu, K. Kusada, T. Yamamoto, T. Toriyama, S. Matsumura, I. Gueye, O. Seo, J. Kim, S. Hiroi, O. Sakata, *et al.*, On the electronic structure and hydrogen evolution reaction activity of platinum group metal-based high-entropy-alloy nanoparticles, Chem. Sci. **11**, 12731 (2020).
[34] M. Liu, Z. Zhang, F. Okejiri, S. Yang, S. Zhou, and S. Dai, Entropy-maximized synthesis of multimetallic nanoparticle catalysts via a ultrasonication-assisted wet chemistry method under ambient conditions, Adv. Mater. Interfaces **6**, 1900015 (2019).
[35] Y. Yao, Z. Huang, P. Xie, S. D. Lacey, R. J. Jacob, H. Xie, F. Chen, A. Nie, T. Pu, M. Rehwoldt, *et al.*, Carbothermal shock synthesis of high-entropy-alloy nanoparticles, Science **359**, 1489 (2018).
[36] X. Huang, B. Zhang, C. Guo, G. Yang, Q. Zhang, S. Li, H. Yu, and F. Peng, Noble-metal high-entropy-alloy tuning the products of electrocatalytic 5-hydroxymethylfurfural oxidation, Sustain. Energy Fuels **7**, 5224 (2023).
[37] D. Wu, K. Kusada, T. Yamamoto, T. Toriyama, S. Matsumura, S. Kawaguchi, Y. Kubota, and H. Kitagawa, Platinum-group-metal high-entropy-alloy nanoparticles, J. Am. Chem. Soc. **142**, 13833 (2020).
[38] S. Sohn, Y. Liu, J. Liu, P. Gong, S. Prades-Rodel, A. Blatter, B. E. Scanley, C. C. Broadbridge, and J. Schroers, Noble metal high entropy alloys, Scr. Mater. **126**, 29 (2017).
[39] S. Nellaiappan, N. K. Katiyar, R. Kumar, A. Parui, K. D. Malviya, K. Pradeep, A. K. Singh, S. Sharma, C. S. Tiwary, and K. Biswas, High-entropy alloys as catalysts for the $CO_2$ and CO reduction reactions: Experimental realization, ACS Catal. **10**, 3658 (2020).
[40] K. M. Urs, N. K. Katiyar, R. Kumar, K. Biswas, A. K. Singh, C. Tiwary, and V. Kamble, Multi-component (Ag–Au–Cu–Pd–Pt) alloy nanoparticle-decorated p-type 2D-molybdenum disulfide ($MoS_2$) for enhanced hydrogen sensing, Nanoscale **12**, 11830 (2020).
[41] P. Hohenberg and W. Kohn, Inhomogeneous electron gas, Phys. Rev. **136**, B864 (1964).
[42] W. Kohn and L. J. Sham, Self-consistent equations including exchange and correlation effects, Phys. Rev. **140**, A1133 (1965).
[43] J. J. Mortensen, A. H. Larsen, M. Kuisma, A. V. Ivanov, A. Taghizadeh, A. Peterson, A. Haldar, A. O. Dohn, C. Schäfer, E. O. Jónsson, *et al.*, GPAW: An open Python package for electronic structure calculations, J. Chem. Phys. **160**, 092503 (2024).
[44] J. Ihm, A. Zunger, and M. L. Cohen, Momentum-space formalism for the total energy of solids, J. Phys. C: Solid State Phys. **12**, 4409 (1979).
[45] See Supplemental Material at http://link.aps.org/supplemental/10.1103/pdjg-z6rb for additional computational details, including the table with differential mixing enthalpy parameters calculated from *ab initio* simulations; root mean square error of the enthalpies of mixing calculated by the DSI and the Miedema model; enthalpy of mixing for refractory binary (MoNb, MoTa, MoW, NbTa, NbW, TaW) and ternary alloys (MoNbTa);

enthalpy of mixing for the binary SiGe system, compared with experimental data from Ref. [60] and Miedema model with parameters from Ref. [64]; enthalpies of mixing for the binary alloys: AuCu, AgCu, AgPt and PdPt; and ternary alloys: AgCuPd, AgCuPt, AgPdPt, AuCuPd, AuCuPt, and AuPdPt; convergence plot of total energy per atom for bulk metals as a function of the energy cutoff.

[46] J. P. Perdew, K. Burke, and M. Ernzerhof, Generalized gradient approximation made simple, Phys. Rev. Lett. **77**, 3865 (1996).

[47] H. J. Monkhorst and J. D. Pack, Special points for Brillouin-zone integrations, Phys. Rev. B **13**, 5188 (1976).

[48] A. Alpatov and S. Paderin, Models and calculations of liquid metallic solutions, Russ. Metall. **2009**, 386 (2009).

[49] M. Sluiter and Y. Kawazoe, Prediction of the mixing enthalpy of alloys, Europhys. Lett. **57**, 526 (2002).

[50] A. Benisek and E. Dachs, Excess enthalpy of mixing of mineral solid solutions derived from density-functional calculations, Phys Chem Minerals **47**, 15 (2020).

[51] T. Abe, B. Sundman, and H. Onodera, Thermodynamic assessment of the Cu-Pt system, J. Phase Equilib. Diffus. **27**, 5 (2006).

[52] P. Subramanian and D. Laughlin, Cu-Pd (Copper-Palladium), J. Phase Equilib. **12**, 231 (1991).

[53] X. Yang and Y. Zhang, Prediction of high-entropy stabilized solid-solution in multi-component alloys, Mater. Chem. Phys. **132**, 233 (2012).

[54] C. M. Rost, E. Sachet, T. Borman, A. Moballegh, E. C. Dickey, D. Hou, J. L. Jones, S. Curtarolo, and J.-P. Maria, Entropy-stabilized oxides, Nat. Commun. **6**, 8485 (2015).

[55] P. Sarker, T. Harrington, C. Toher, C. Oses, M. Samiee, J.-P. Maria, D. W. Brenner, K. S. Vecchio, and S. Curtarolo, High-entropy high-hardness metal carbides discovered by entropy descriptors, Nat. Commun. **9**, 4980 (2018).

[56] J. Gild, J. Braun, K. Kaufmann, E. Marin, T. Harrington, P. Hopkins, K. Vecchio, and J. Luo, A high-entropy silicide: $(Mo_{0.2}Nb_{0.2}Ta_{0.2}Ti_{0.2}W_{0.2})Si_2$, J. Materiomics **5**, 337 (2019).

[57] M. C. Folgueras, Y. Jiang, J. Jin, and P. Yang, High-entropy halide perovskite single crystals stabilized by mild chemistry, Nature (London) **621**, 282 (2023).

[58] L. Lin, K. Wang, A. Sarkar, C. Njel, G. Karkera, Q. Wang, R. Azmi, M. Fichtner, H. Hahn, S. Schweidler, and B. Breitung, High-entropy sulfides as electrode materials for Li-ion batteries, Adv. Energy Mater. **12**, 2103090 (2022).

[59] J. Cavin, A. Ahmadiparidari, L. Majidi, A. S. Thind, S. N. Misal, A. Prajapati, Z. Hemmat, S. Rastegar, A. Beukelman, M. R. Singh, *et al.*, 2D high-entropy transition metal dichalcogenides for carbon dioxide electrocatalysis, Adv. Mater. **33**, 2100347 (2021).

[60] C. Bergman, R. Chastel, and R. Castanet, Thermodynamic investigation on the Si-Ge binary system by calorimetry and Knudsen cell mass spectrometry, J. Phase Equilib. **13**, 113 (1992).

[61] K. Fitzner and O. Kleppa, Thermochemistry of binary and ternary noble metal alloys: The systems Cu-Ce, Ag-Ce, Au-Ce, Cu-Ag-Au, and Ce-Ag-Au, Metall Trans A **24**, 1827 (1993).

[62] D. B. Miracle and O. N. Senkov, A critical review of high entropy alloys and related concepts, Acta Mater. **122**, 448 (2017).

[63] M. S. Mousavi, R. Abbasi, and S. F. Kashani-Bozorg, A thermodynamic approach to predict formation enthalpies of ternary systems based on Miedema's model, Metall. Mater. Trans. A **47**, 3761 (2016).

[64] A. Takeuchi and A. Inoue, Classification of bulk metallic glasses by atomic size difference, heat of mixing and period of constituent elements and its application to characterization of the main alloying element, Mater. Trans. **46**, 2817 (2005).